**ChemistryOpen**

Research Article
doi.org/10.1002/open.202100261

**Chemistry Europe**
European Chemical Societies Publishing

www.chemistryopen.org

# A DNA Biosensor Based on a Raspberry-like Hierarchical Nano-structure for the Determination of the Anticancer Drug Nilotinib

Mohammad Mehdi Moarefdoust,[a, b] Shohreh Jahani,*[c] Mehran Moradalizadeh,[a] Mohammad Mehdi Motaghi,[a] and Mohammad Mehdi Foroughi*[a]

It is crucial to design fast, sensitive and affordable deoxyribonucleic acid (DNA) recognition instruments, and elucidate changes in DNA structure, for studying the interaction between DNA and chemotherapy drugs. Therefore, a DNA biosensor, based on a carbon paste electrode (CPE), modified with raspberry-like indium(III)/nickel oxide hierarchical nano-structures ($In^{3+}$/NiO RLHNSs) was constructed. An electrochemical readout should then give information on the interactions between anticancer drugs and double-stranded (ds)-DNA. The morphology as well as the electrochemical description of this new biosensor is described. Based on experimentally determined optimal conditions, ds-DNA modified with $In^{3+}$/NiO RLHNSs/CPE was used to evaluate the binding interaction of nilotinib, as an anti-cancer drug, with DNA through differential pulse voltammetry (DPV), UV-Vis spectroscopy, viscosity measurements and a computational docking process. The analyses indicated the linearity of the guanine oxidation signal at nilotinib concentration is given between 0.01 and 50.0 μM, with the limit of detection (LOD) equal to 0.62 nM. Additionally, the equilibrium constant (K) for the binding was determined to $1.5 \times 10^4 \, M^{-1}$. Through the quantitative measurement of nilotinib in serum samples with a high recovery rate of 101.3–98.0%, the applicability of this approach was demonstrated. As a whole, this DNA biosensor may be promising for various bio-interactions.

## Introduction

Chronic myelogenous leukemia (CML), also called chronic myeloid leukemia, has been introduced as one of the cancers affecting white blood cells (WBCs), and described by the greater and unregulated growth of myeloid cells in the bone marrow and their accumulation in the blood. This condition can be cured using targeted drugs, known as tyrosine-kinase inhibitors (TKIs).[1] As one of such TKIs, 4-methyl-N-[3-(4-methyl-1H-imidazol-1-yl)-5-(trifluoromethyl)phenyl]-3-[(4-pyridin-3-ylpyri-midin-2-yl)amino]benzamide – nilotinib – as well as its hydrochloride and its HCl monohydrate are available, the latter marketed under the brand name Tasigna. Nilotinib, employed to cure CML,[2,3] is also utilized for treating cases of Philadelphia (Ph) chromosome-positive CML. Parise et al. described an HPLC-mass spectrometry (MS) method for determination of nilotinib in plasma and serum.[4] Furthermore, simultaneous determination of nilotinib with other anti-chronic myeloid leukemia drugs using solid phase extraction and ultra-performance liquid chromatography-tandem mass (UPLC-MS/MS),[5] HPLC-MS,[6] HPLC-MS/MS,[7,8] and HPLC-UV[9] have been reported.

Even though such techniques have been considered sensitive, they suffer from multiple caveats, like complicated devices – only available in selected laboratories – and laborious sample pre-treatment.[10–14]

Compared to the above-mentioned techniques, electrochemical procedures can be acceptable alternatives to analyze drugs because of their utility, simplification, and rapidness as well as easier miniaturization.[15–20] Moreover, the electrochemical examination of deoxyribonucleic acid (DNA)-drug interactions may be a fast and affordable technique to detect drugs. It is notable that electrochemical DNA biosensors have been made based on the immobilization of the nucleic acid recognition layer on the electrochemical transducer. In addition, the nucleic acid recognition layer has been used to detect modifications in the DNA structure in the course of intercalations with the DNA-binding molecules.[21] Remarkably, evaluations based on DNA interactions will be very valuable to know the mechanisms of several drug compounds, and, in turn, to devise novel DNA biosensors. Electrochemical DNA biosensors

[a]  M. M. Moarefdoust, Dr. M. Moradalizadeh, Dr. M. M. Motaghi, Dr. M. M. Foroughi
Department of Chemistry
Kerman Branch
Islamic Azad University
Kerman (Iran)
E-mail: foroughi@iauk.ac.ir

[b]  M. M. Moarefdoust
Department of Chemistry
Zarand Branch
Islamic Azad University
Zarand (Iran)

[c]  Dr. S. Jahani
Noncommunicable Diseases Research Center
Bam University of Medical Sciences
Bam (Iran)
E-mail: shohre_jahani@yahoo.com

**ChemistryOpen**

Research Article
doi.org/10.1002/open.202100261

**Chemistry
Europe**
European Chemical
Societies Publishing

can be produced through DNA immobilization at the electrode surface.[22–24] Nevertheless, electrochemical procedures face difficulties in detecting nucleic bases due to slower electron-transfer kinetics, as well as higher overpotential and over-lapping of the respective oxidation peaks. To resolve such problems, it is useful to apply chemically modified electrodes.[25,26] Accordingly, nano-materials (NMs) are usually utilized for biosensor modification because of their greater catalytic features and higher electrical conductivity. Conse-quently, more active sites and considerable functional groups at the surface of NMs result in higher activities for catalysis and absorption.[27–33]

Nickel oxide (NiO), a broadband gap (3.6–4.0 eV) p-type semiconductor with high thermal stability and specific optical, electrical, and magnetic features, has been identified as one of the desirable candidates for different utilizations such as sensing (e.g., for non-enzymatic glucose sensors), use as absorbent, as a battery cathode, a magnetic material, a catalyst, and in super-capacitor electrodes.[34,35] Specifically, the prepara-tion of NiO nano-flowers preparation has been considered interesting because of the resulting unique physicochemical characteristics compared with conventional nano-crystallites. By introducing rare-earth and transition metals, it is possible to adjust the electrical, morphological, optical, as well as magnetic characteristics of the metal oxide nano-structures (NSs).[36]

To the best of the authors' knowledge, no study has so far reported on nilotinib determination with the application of electrochemical biosensors. Next to addressing this gap, the present study also introduces a simplified direct method to reproducibly synthesize a three-dimensional (3D) raspberry-like $In^{3+}$/NiO hierarchical NS ($In^{3+}$/NiO RLHNS) for the first time. They have been studied for their morphological as well as structural features. A simplified $In^{3+}$/NiO RLHNSs-modified carbon-paste electrode (CPE) ($In^{3+}$/NiO RLHNSs/CPE) was as-sembled, and double-stranded (ds)-DNA immobilization on the surface of the $In^{3+}$/NiO RLHNSs/CPE was achieved through an adsorption technique in acetate buffer solution (ABS) at pH 4.8. This new DNA biosensor (i.e., the ds-DNA/$In^{3+}$/NiO RLHNSs/CPE) was initially utilized to determine nilotinib electrochemi-cally.

Since the electrochemical detection of nilotinib is based on observing modifications in the oxidation signal of guanine, consequently, the interaction mechanisms of ds-DNA with nilotinib were explored through UV-Vis spectroscopy, differ-ential pulse voltammetry (DPV), a computational docking process, and viscosity measurements. This new DNA biosensor was finally utilized to detect nilotinib in human blood serum and urine samples.

## Results and Discussion

### Characterization of $In^{3+}$/NiO RLHNSs

The XRD spectra from $In^{3+}$/NiO NPs are shown in Figure S1, indicating 2θ values of 79.69°, 73.11°, 62.40°, 43.57° and 37.30° related to lattice planes of (002), (021), (111), (200) and (001),

respectively, in line with the Joint Committee of Powder Diffraction Standards (JCPDS, No. 03-065-6920).[37] Moreover, the diffraction signals have shifted clearly towards lower angle, signifying minor doping of $In^{3+}$ into the NiO lattice. This can happen since the ionic radius of $In^{3+}$ (0.94 Å) is larger than that of $Ni^{2+}$ (0.72 Å), making the lattice expand in $In^{3+}$-doped NiO crystals. Therefore, the replacement of $Ni^{2+}$ in the lattice with $In^{3+}$ may predict partial changes, which do however not cause any alterations in the crystal lattice.

The morphological and micro-structural properties of as-produced $In^{3+}$/NiO were explored by FESEM (Figures 1a, b). The FESEM image with lower magnification (Figure 1a) reveals the microsphere morphology for $In^{3+}$/NiO with the mean diameter of approximately 250 nm. The FESEM image with higher magnification (Figure 1b) shows the more obvious morphology, the microspheres having uneven surfaces with a mass of fine NPs (20–40 nm) and, thus, raspberry-like shape.

The $In^{3+}$/NiO RLHNSs composite was additionally explored using elemental mapping (EM) and EDX analysis (Figure S2), the results of which confirmed the presence of O, In and Ni in the products. The content of In from the EDX spectra express the outputs of $In^{3+}$-doped NiO nano-structures. In fact, the EM shows the elements scattered on the surface (Figure S2), as shown by the homogenous distribution of In, O and Ni.

### Characterization of the Modified Electrode

To characterize the modified electrode, the cyclic voltammo-gram (CV) of the $[Fe(CN)_6]^{3-/4-}$ redox couple, as an index, was recorded to immobilize DNA at the surfaces of bare CPE, NiO RLHNSs/CPE, $In^{3+}$/NiO RLHNSs/CPE, and ds-DNA/$In^{3+}$/NiO RLHNSs/CPE. With regard to the data in Figure 2(a), the redox peak current as well as the reversibility at the NiO RLHNSs/CPE (Curve b) augmented in comparison with that of the un-modified electrode (Curve a). This is probably caused by the faster electron transfer and the bigger surface area of the NiO RLHNSs/CPE, leading to a higher current response. Moreover, for the $In^{3+}$/NiO RLHNSs/CPE (Curve c), the peak potential separation ($\Delta E_p$) diminished and the peak current considerably enhanced, as compared with the CPEs and the NiO RLHNSs/CPE. These outputs can be attributed to the synergic impact of NiO and $In^{3+}$, resulting in the increased modified electrode function like faster electron transfer rate, higher conductivity, as well as acceptable anti-fouling feature. Once DNA was immobi-lized, at the surface of the $In^{3+}$/NiO RLHNSs/CPE, two anodic and cathodic peak currents remarkably reduced after enhancing the peak-to-peak potential separation (Curve d). The outputs indicated the resistance of the phosphate groups with the negative charge of the immobilized DNA for the access of the redox couple to the electrode. In addition to this electrostatic repulsion, the immobilized ds-DNA may function as one of the physical blockers to transfer electron. Hence, the current reduced. Finally, DNA immobilization was obtained at the surface of the $In^{3+}$/NiO RLHNSs/CPE.

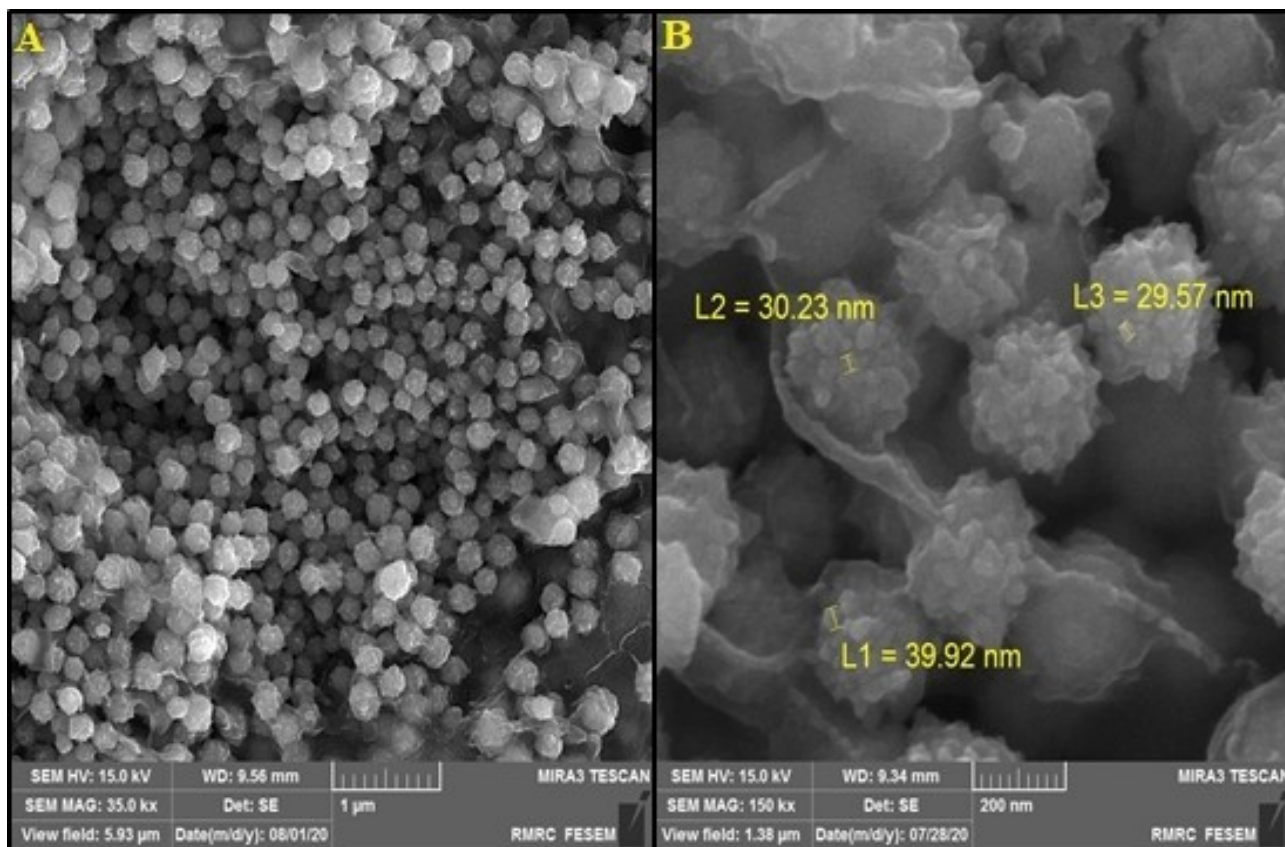It is widely accepted that EIS is one of the flexible techniques for revealing the impedance property of electrode/

**ChemistryOpen**

Research Article
doi.org/10.1002/open.202100261

**Chemistry Europe**
European Chemical
Societies Publishing

**Figure 1.** (A) FESEM image and (B) high-resolution FESEM image of $In^{3+}$/NiO RLHNSs.

solution interface with the use of a redox probe, $[Fe(CN)_6]^{3-/4-}$. In general, the semi-circle diameter in a Nyquist plot can be used to analyze the charge transfer resistance ($R_{ct}$). Figure 2(b) represents the Nyquist charts of the impedance spectra, registered on the CPE, in the course of the surface layer assembly. As shown in Figure 2(b), the electron $R_{ct}$-value for the bare CPE equaled 463 Ω (Curve a), and declined significantly to 283 Ω (Curve b) for the NiO RLHNSs/CPE and 108 Ω (Curve c) for the $In^{3+}$/NiO RLHNSs/CPE, which verified an acceptable electrical conductivity of the provided film, reflecting more robust capability of the electron transfer of the redox ions to the surface of electrode. Once ds-DNA has been immobilized on the $In^{3+}$/NiO RLHNSs/CPE (Curve d), a gradual enhancement in the $R_{ct}$-value (793 Ω) was registered, denoting lower abilities to transfer the electrons at the electrode surface, largely caused by the non-conductive behaviors of ds-DNA, which created an obstacle for $[Fe(CN)_6]^{3-/4-}$ ions in terms of reaching the electrode.

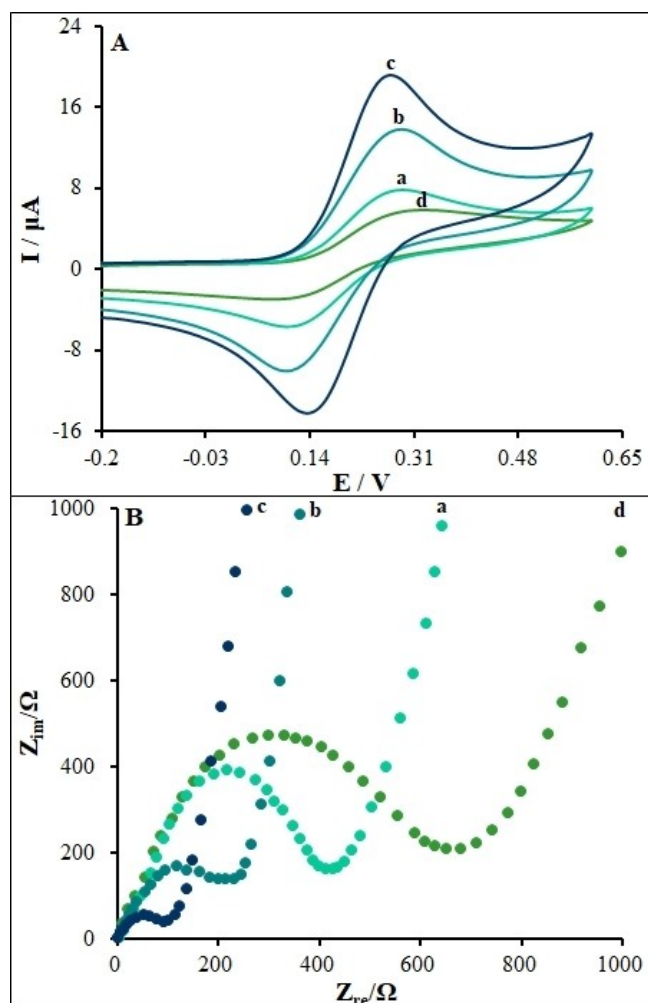The electroactive surface areas of bare CPE, NiO RLHNSs/CPE and $In^{3+}$/NiO RLHNSs/CPE were determined from cyclic voltammograms of 0.5 mM $[Fe(CN)_6]^{3-/4-}$ in 0.1 M KCl at various scan rates (Figure S3) using the Randles-Ševčík equation [Eq. (1)].[38,39]

$$I_p = \pm(2.69 \times 10^5)\, n^{3/2}\, A\, D^{1/2}\, C\, \nu^{1/2} \qquad (1)$$

where D represents the diffusion coefficient ($cm^2 s^{-1}$), A stands for the electrode surface area ($cm^2$), C stands for the $[Fe(CN)_6]^{3-/4-}$ (0.5 mM) concentration, n shows the number of electrons consisted in the process (n = 1), $I_p$ stands for the intensity of peak current (A), and $\nu$ denotes the scan rate ($V s^{-1}$). The electroactive surface areas for the $In^{3+}$/NiO RLHNSs/CPE, NiO RLHNSs/CPE and bare CPE are calculated to 0.23, 0.18 and 0.083 $cm^2$, respectively. The obtained outcomes demonstrate that $In^{3+}$/NiO RLHNSs/CPE can provide a larger electroactive area and making it a promising material, which can promote the sensitivity together with electron transfer ability of the electrodes.

**Absorbing ds-DNA on the $In^{3+}$/NiO RLHNSs/CPE**

In this step, ds-DNA was immobilized on the $In^{3+}$/NiO RLHNSs/CPE surface using the direct adsorption method. Figure 3 displays the intensities of the guanine oxidation signals of the ds-DNA/$In^{3+}$/NiO RLHNSs/CPE electrodes at a ds-DNA concentration range between 5 and 25 mg L$^{-1}$. An enhanced peak current of the guanine oxidation was observed as the ds-DNA concentration was elevated to 17.5 mg L$^{-1}$, and consequently leveled off, Figure 3(a). Hence, the optimal ds-DNA concentration was chosen as 17.5 mg L$^{-1}$. A significant factor to immobilize ds-DNA was further proposed to be the absorption time.

**ChemistryOpen**

Research Article
doi.org/10.1002/open.202100261

**Chemistry
Europe**
European Chemical
Societies Publishing

**Figure 2.** (A) Cyclic voltammograms of 5 mM $[Fe(CN)_6]^{3-/4-}$ in 0.1 M KCl: (a) CPE, (b) NiO RLHNSs/CPE (c) $In^{3+}$/NiO RLHNSs/CPE, (d) ds-DNA/$In^{3+}$/NiO RLHNSs/CPE. Scan rate: 50 mV s$^{-1}$; (B) Nyquist plots of (a) CPE, (b) NiO RLHNSs/CPE (c) $In^{3+}$/NiO RLHNSs/CPE, (d) ds-DNA/$In^{3+}$/NiO RLHNSs/CPE in 0.1 M KCl containing 5.0 mM $[Fe(CN)_6]^{3-/4-}$.

Figure 3(b) demonstrates the intensities of the guanine oxidation signal at the ds-DNA/$In^{3+}$/NiO RLHNSs/CPE for 17.5 mg L$^{-1}$ of ds-DNA at various accumulation time-points (50–300 s). As seen, the intensities of the guanine oxidation signal were enhanced for an absorption time of 150 s and subsequently leveled off. Hence, 150 s was chosen as the optimal absorption time of ds-DNA to procure the ds-DNA/$In^{3+}$/NiO RLHNSs/CPE.

### Electrochemical Analysis of the Interaction between Nilotinib and ds-DNA at the $In^{3+}$/NiO RLHNSs/CPE

The optimal conditions for the interaction between ds-DNA and nilotinib were also determined by investigating the impact of interaction time and nilotinib concentration. Therefore, the interaction time of nilotinib with ds-DNA at the $In^{3+}$/NiO RLHNSs/CPE was initially optimized. With regard to Figure 3(c), upon the interaction with nilotinib, the guanine oxidation signal declined up to 200 s, and it nearly leveled off from 200 to 225 s.

Thus, 200 s was chosen as an optimum time to induce the interaction between nilotinib and ds-DNA.

In the next step, the effects of the nilotinib concentration on the DPV signals were assessed in the presence and absence of ds-DNA within a concentration range of 0–22.5 μM. Figure 4 is a representation of the DPVs of ds-DNA at the $In^{3+}$/NiO RLHNSs/CPE electrode for diverse concentrations of nilotinib. As observed, the increased concentration of nilotinib declined the oxidation peak current for the guanine signal, and thus lower guanine oxidation peak current could be assigned to the binding of nilotinib to ds-DNA. Therefore, this rising trend can be justified as one of the probable damages to the oxidized groups of electroactive bases of DNA, whereas nilotinib interacted with ds-DNA at the surface of the $In^{3+}$/NiO RLHNSs/CPE.[40,41] In addition, the negative or positive shifts in the potential of the guanine oxidation peak demonstrated the binding form, through intercalation or electrostatic binding.[42] As seen in Figure 4, there is no measurable shift in the oxidation peak potential of guanine once nilotinib was added to it. Thus, the binding mode of nilotinib to ds-DNA cannot be assumed as an intercalative binding or an electrostatic interaction.
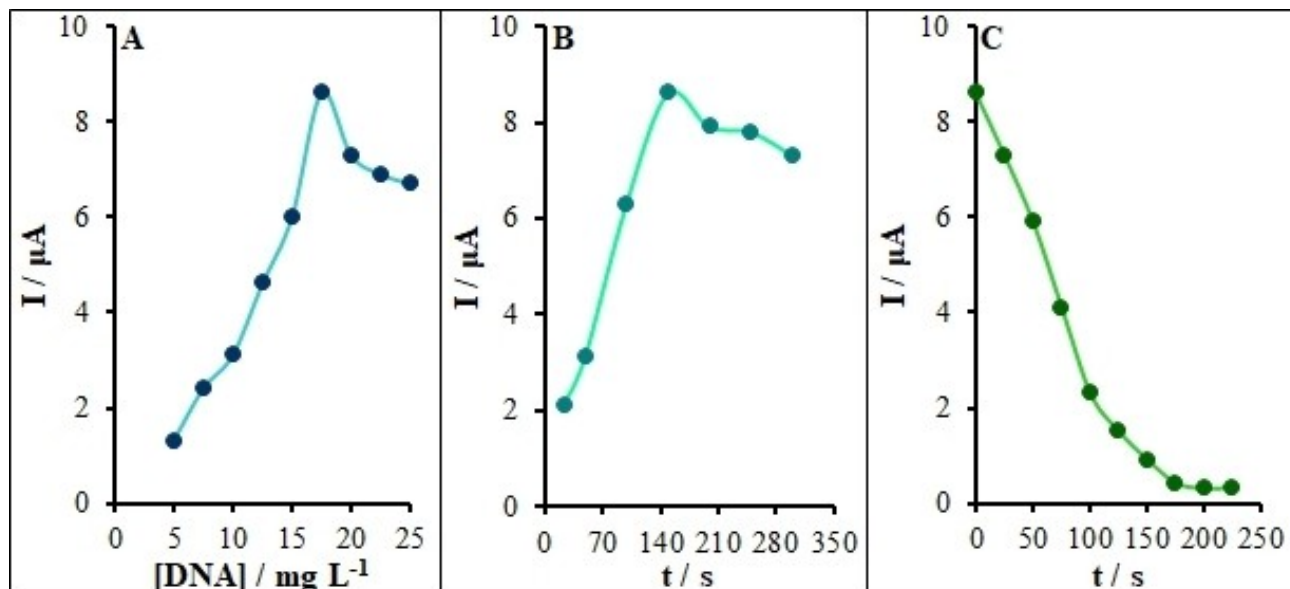
The ds-DNA/$In^{3+}$/NiO RLHNSs/CPE was used for the quantitative determination of nilotinib based on the DPV, whose responses of the ds-DNA/$In^{3+}$/NiO RLHNSs/CPE for the increasing concentration of nilotinib, under optimum experimental conditions, are displayed in Figure 5(a). With regard to Figure 5(b), the oxidation peak current of guanine showed linearity with the concentration of nilotinib within a range between 0.01 and 50.0 μM, and a linear equation of $I(\mu A) = 0.1431 \times C + 0.0961$ with $R^2 = 0.9992$ (n = 3) was fitted, with C representing tge nilotinib concentration in μM. Finally, the limit of quantitation (LOQ) as well as the LOD from the calibration curve equaled 2.08 nM and 0.62 nM, respectively, and consequently the LOD and LOQ values verified the modified electrode sensitivity, computed by Equation (2):[43]

$$LOD = 3\,s/m, \quad LOQ = 10s/m \tag{2}$$

Where $s$ represents the current standard deviation (SD) (three runs) for the minimum concentration of the linearity range and $m$ refers to the slope of the respective calibration curve. As listed in Table 1,[44–49] the sensor indicates lower LOD, good linear dynamic range, and a comparable or even greater sensitivity (seen from the calibration curve slope) in comparison with other reported nilotinib methods frp, recent studies. The wonderful outcomes from the ds-DNA/$In^{3+}$/NiO RLHNSs/CPE can be attributed to the excellent electron transfer and the high effective surface area of the $In^{3+}$/NiO RLHNSs, by which high sensitivity was conducted to a synergic influence towards nilotinib detection.

### Repeatability, Reproducibility and Stability

To evaluate the accuracy of this procedure, repeatability and reproducibility were investigated. For this, the guanine oxidation signal at a similar electrode was measured to evaluate the

**ChemistryOpen**

Research Article
doi.org/10.1002/open.202100261

**Chemistry
Europe**
European Chemical
Societies Publishing

**Figure 3.** (A) The oxidation signal plot of guanine vs. ds-DNA concentration (2.0–25.0 mg L$^{-1}$); (B) the oxidation signal plot of guanine in different accumulation time of ds-DNA (50–300 s); (C) influence of incubation time of 50.0 μM nilotinib in ABS (0.1 M, pH 4.8) on the response of ds-DNA/In$^{3+}$/NiO RLHNSs/CPE.
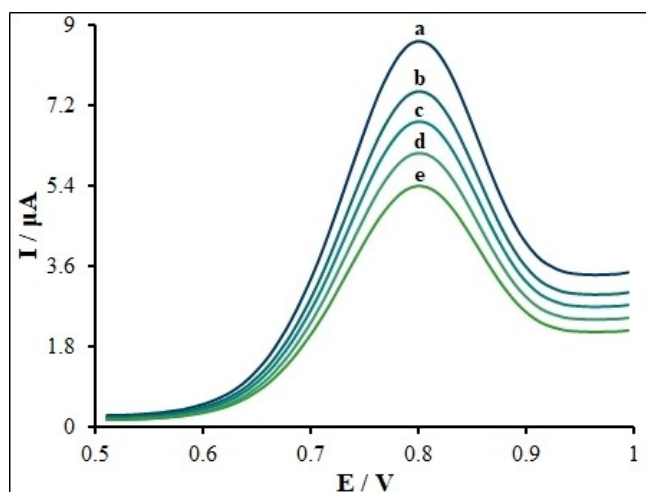


**Figure 4.** Differential pulse voltammograms of guanine after the interaction between 0.0, 5.0, 15.0, and 25.0 μM nilotinib in ABS (0.1 M, pH 4.8) (curves a–d, respectively) and ds DNA at ds-DNA/In$^{3+}$/NiO RLHNSs/CPE.
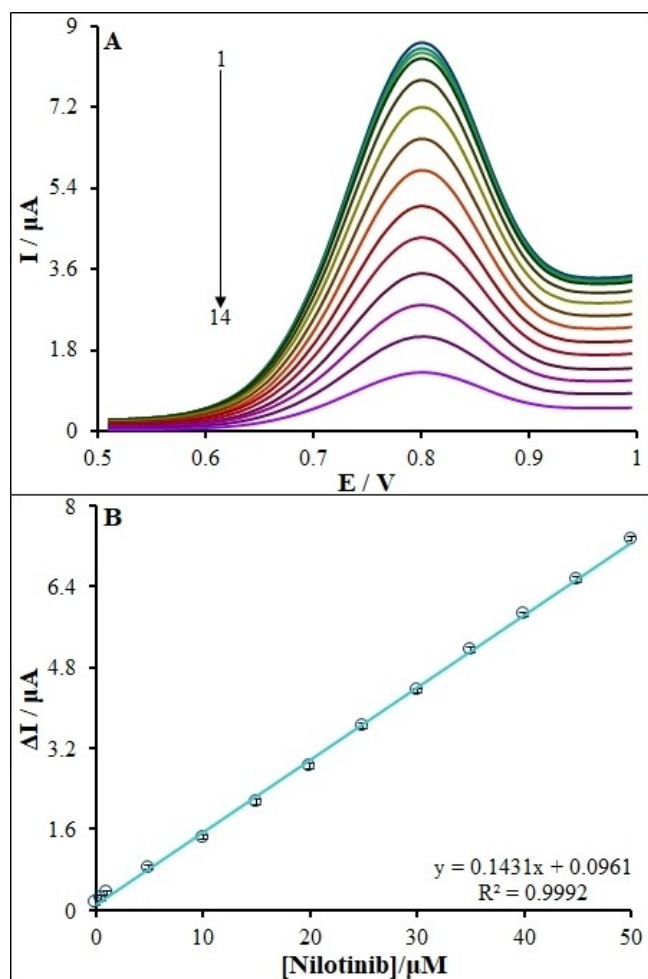
repeatability of the ds-DNA-adsorbed modified electrode. The relative SD (RSD) of five frequent measurements equaled 2.46% and the ds-DNA/In$^{3+}$/NiO RLHNSs/CPE and reproducibility was computed from the alterations in the oxidation peak current for the guanine signal, obtained through five distinct electrodes. From this, the RSD-value of reproducibility was calculated to 2.28%.

In addition, the stability of the ds-DNA/In$^{3+}$/NiO RLHNSs/ CPE was tested. When the ds-DNA/In$^{3+}$/NiO RLHNSs/CPE was kept in 0.1 M PBS after voltammetric measurements, the guanine oxidation current signals kept nearly stable in the first 10 days and decreased about 2.4% of its initial response after 30 days, indicating good stability of the In$^{3+}$/NiO RLHNSs-modified CPE.

### Interference Study

The effect of foreign species on the guanine signals was analyzed by DPV in the presence of 10.0 μM nilotinib to assess the selectivity of the sensor. In addition, the maximum interfering material concentration, resulting in errors under ±5% to detect guanine, was described as the tolerance limit. With regard to these analyses, up to a 500-fold excessive uric acid ($C_5H_4N_4O_3$), sucrose ($C_{12}H_{22}O_{11}$), citrate acid ($C_6H_8O_7$), ascorbic acid ($C_6H_8O_6$), epinephrine ($C_9H_{13}NO_3$), dopamine ($C_8H_{11}NO_2$), L-tyrosine ($C_9H_{11}NO_3$), as well as folic acid ($C_{19}H_{19}N_7O_6$) had no impact on the guanine oxidation signal (Figure 6). Finally, the ds-DNA/In$^{3+}$/NiO RLHNSs/CPE biosensor was found suitable for nilotinib determination.

**Table 1.** Comparison of the efficiency of different methods used in detection of nilotinib.

| Method | LOD | LDR | Ref |
|---|---|---|---|
| Selective extraction | 0.002 mg L$^{-1}$ | 0.01–10.0 mg L$^{-1}$ | [44] |
| High-performance liquid chromatography | – | 250–5000.0 ng mL$^{-1}$ | [45] |
| High-performance liquid chromatography | 0.06 μM | 0.20–10.0 μM | [46] |
| Spectrofluorometric | 0.025 μg mL$^{-1}$ | 0.1–1.0 μg mL$^{-1}$ | [47] |
| Ultra-high-performance liquid chromatography | – | 2.5–250.0 μg L$^{-1}$ | [48] |
| Voltammetry | 6.33 nM | 0.02–2.0 μM | [49] |
| Voltammetry | 0.62 nM | 0.01–50.0 μM | This work |

**ChemistryOpen**

Research Article
doi.org/10.1002/open.202100261

**Chemistry**
**Europe**
European Chemical
Societies Publishing

**Figure 5.** Voltammograms of ds-DNA/In$^{3+}$/NiO RLHNSs/CPE for different concentrations of nilotinib in ABS (0.1 M, pH 4.8). From top to bottom (1–14), 0.0, 0.01, 0.5, 1.0, 5.0, 10.0, 15.0, 20.0, 25.0, 30.0, 35.0, 40.0, 45.0 and 50.0 μM; (B) dependence of the net oxidation guanine current (different between guanine current in the absence and presence of nilotinib) vs. concentration of nilotinib.

## UV-Visible Absorption Analyses

Absorption spectrophotometry was utilized to clarify the interactions of nilotinib with ds-DNA. UV-Visible absorption spectra of the ds-DNA/nilotinib system and ds-DNA were recorded in ABS at a pH of 4.8. The results showed the absorption peak of nilotinib at nearly 264 nm that approximated to the absorption peak of ds-DNA at 260 nm, as illustrated in Figure 7(a). When ds-DNA (5–40 mg L$^{-1}$) was added to the fixed concentration of nilotinib (30 mg L$^{-1}$), the absorption spectrum of nilotinib at 264 nm (that is, hyperchromism) with a slight blue shift enhanced, Figure 7(a). According to the outputs, nilotinib interacted with ds-DNA. Additionally, the total absorption intensity of free nilotinib and free ds-DNA were lower than the ds-DNA-nilotinib complexes. From previous studies, the binding of the small molecules to ds-DNA by intercalation led to hyperchromism and considerable red shift ($\geq$ 15 nm), whereas outside binding molecules showed a smaller red shift ($\leq$ 8 nm).[50] Regarding the groove-binding mole-

cules binding on the DNA external surface, smaller or no bathochromism was commonly seen.[51] The UV-Vis spectrum outputs of nilotinib-DNA complex also suggested that nilotinib had possible interaction with ds-DNA through the groove binding. According to the modifications of the absorbance spectra of nilotinib by binding to ds-DNA, it is possible to determine the binding constant (K) with Equation (3):

$$A_0/(A - A_0) = \varepsilon_C/(\varepsilon_{H\text{-}C}\text{-}\varepsilon_C) + 1/K[DNA] \tag{3}$$
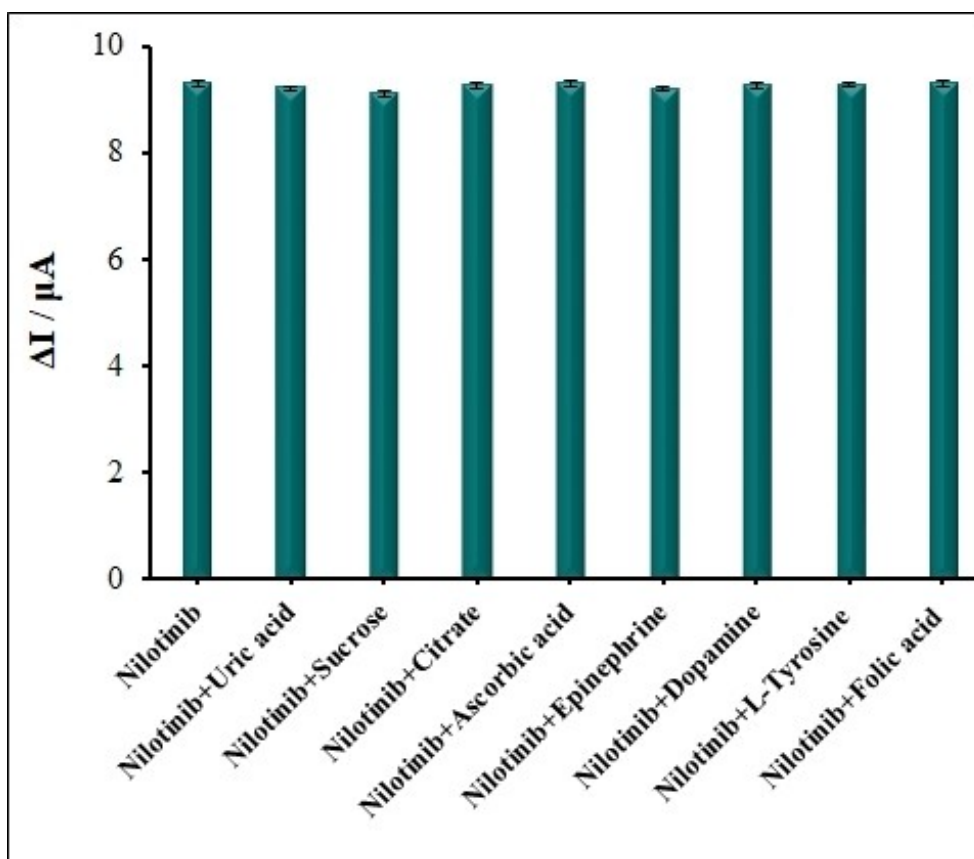
in which K refers to the binding constant; $A_0$ and $A$ represent the absorbance value of the medicine and its complex with ds-DNA; $\varepsilon_C$ and $\varepsilon_{H\text{-}C}$ stand for the adsorption coefficient of the medicine and nilotinib/ds-DNA complex. Therefore, K can be calculated from the ratio of intercept to slope of $A_0$/(A–A$_0$) versus 1/[ds-DNA] plot, as shown in Figure 7(b). In our case, K-value for the nilotinib/ds-DNA interactions equaled $1.5 \times 10^4$ M$^{-1}$. Hence, the kind of interaction of ds-DNA with nilotinib is likely taking place through the groove-binding mode.[52]

## Viscosity Examinations

One of the helpful techniques to determine the binding mode between the small molecules as well as DNA has been proposed to be viscosity measurements that have sensitivity to changes in the length of the double helix, as a prominent experiment of the classical intercalative binding mode. In this sense, a classical intercalative binding of small molecules usually results in the increased viscosity of DNA solution. Reversely, non-intercalation binding like electrostatic or groove bindings can only partly influence DNA viscosity because they do not make changes in the axial length of ds-DNA during the binding.[53] With regard to Figure 8, the relative viscosity of ds-DNA exhibits only minor changes, showing that the binding mode of nilotinib with ds-DNA is not an intercalative interaction. The above behavior reflects that a non-intercalative and probably a groove binding must lead to an interaction mode of nilotinib with ds-DNA.

## Docking Studies

Docking has been thus far performed for examining the optimal interaction site and the most acceptable compound conformation on DNA with minimum energy.[54] The lowest binding energy as well as $K_i$ to interact between DNA and nilotinib respectively equaled $-15.21$ kcal mol$^{-1}$ and 7.1 pM. Further analyses revealed nilotinib stability at the DNA minor groove through five hydrogen bonds with hydrophobic and nucleotide interactions (Figure 9). In addition, hydrogen bonds significantly contributed to the DNA-nilotinib interactions. Notably, hydrogen bonds entailed hydrogen (H)$_{22}$ of guanine 16 (DG16) interacted with nitrogen (N)$_8$ from nilotinib. Afterwards, (H)$_{42}$ of nilotinib interacted with (O)$_{4'}$ from adenine 17 (DA17) and (H)$_4$ of nilotinib interacted with (O)$_{4'}$ from thymine 19 (DT19). Furthermore, (O)$_4$ of nilotinib established a hydrogen bond with

**ChemistryOpen**

Research Article
doi.org/10.1002/open.202100261

**Chemistry**
**Europe**

European Chemical
Societies Publishing

**Figure 6.** The oxidation current diagram of ds-DNA/In$^{3+}$/NiO RLHNSs/CPE in the presence of 10.0 μм nilotinib in ABS (0.1 м, pH 4.8) and other investigated interferences.

(H)$_3$ from adenine 18 (DA18) and (N)$_{11}$ of nilotinib interacted with (H)$_3$ from adenine 6 (DA6). Based on the docking process outputs, nilotinib may interact with the bases in the DNA minor groove.

**Analyzing Real Samples**

To investigate the precision of this new technique, the ds-DNA/In$^{3+}$/NiO RLHNSs/CPE was utilized for analyzing nilotinib in the human blood serum and urine samples. A specific volume of nilotinib was poured into the samples and its content was measured with the use of the ds-DNA/In$^{3+}$/NiO RLHNSs/CPE through the standard addition method. Table 2 reports the outputs. As seen, the recovery value of the human blood serum and urine samples are at the ranges from 98.0 to 101.3%. To analyze the biological samples, the standard addition method was employed for determining the nilotinib concentration, which spiked into the test sample (Table 2). The outputs also demonstrated the utility of this new electrochemical biosensor based on the ds-DNA/In$^{3+}$/NiO RLHNSs/CPE to detect nilotinib in the human blood serum and urine samples.
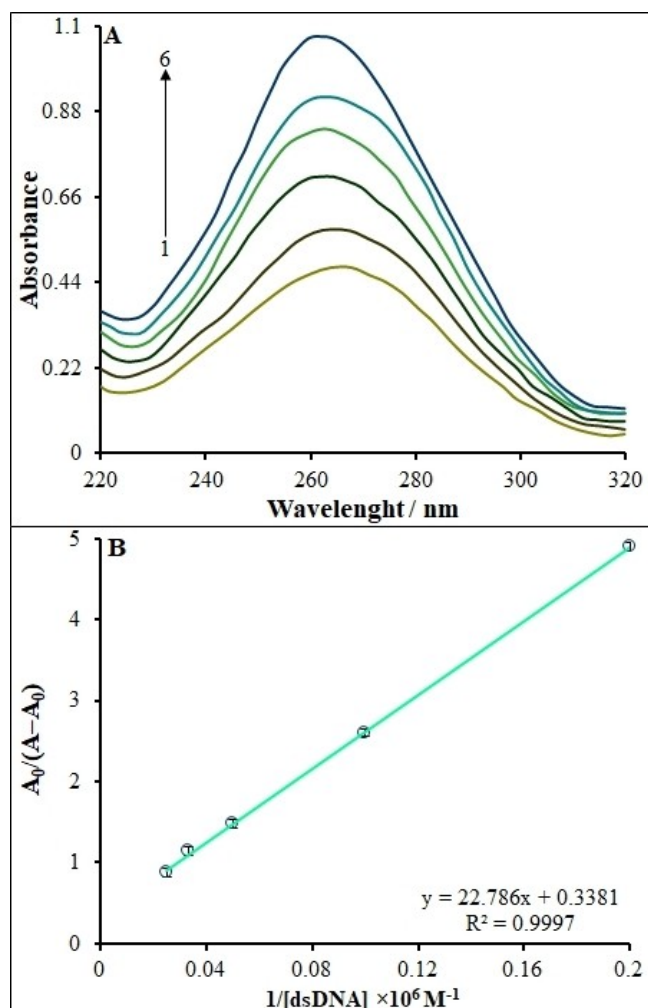
**Table 2.** Application of ds-DNA/In$^{3+}$/NiO RLHNSs/CPE for concurrent determination of nilotinib in human blood serum and urine samples. All concentrations given in μм.

| Sample | Spiked | Found[a] | Recovery [%] |
|---|---|---|---|
| Human blood serum | ND[b] | – | – |
|  | 5.0 | 4.9±2.3 | 98.0 |
|  | 7.5 | 7.6±1.6 | 101.3 |
| Urin | ND[b] | – | – |
|  | 10.0 | 10.1±2.8 | 101.0 |
|  | 20.0 | 19.8±2.1 | 99.0 |

[a] Mean±standard deviation for n=5; [b] not detected.

**Conclusion**

In this paper, electrochemical determination of nilotinib through guanine oxidation using ds-DNA/In$^{3+}$/NiO RLHNSs/CPE was investigated. The ds-DNA/In$^{3+}$/NiO RLHNSs/CPE exhibited higher electrocatalytic activity for determination of nilotinib, which is attributable to superior conductivity and larger surface area of the DNA-biosensor. The results showed reasonable repeatability, reproducibility and stability of this novel biosensor to detect nilotinib with a wide linear range of 0.01–50.0 μм, a low LOD of 0.62 nм, S/N=3, as well as very good selectivity in the presence of interference. Life time of the ds-DNA/In$^{3+}$/NiO RLHNSs/CPE is 70 measurements with current loss less than 8%.

**ChemistryOpen**

Research Article
doi.org/10.1002/open.202100261

**Chemistry Europe**
European Chemical
Societies Publishing

**Figure 7.** (A) UV-vis absorption spectra of nilotinib (15.0 μM) in the absence and presence of the ds-DNA, the numbers 1–6 correspond to 5.0, 10.0, 20.0, 30.0 and 40.0 μM. (B) The plot of $A_0/A-A_0$ vs. 1/[ds-DNA].
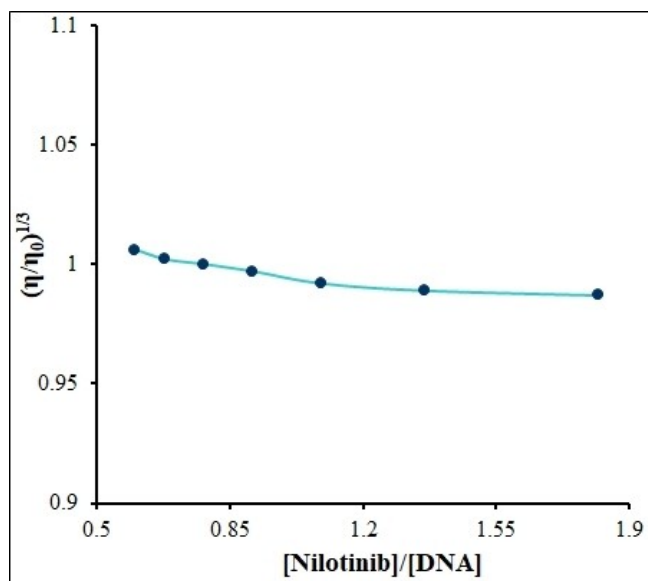


**Figure 8.** Effect of increasing amount of nilotinib on the relative viscosity of ds-DNA in ABS (pH 4.8).

This DNA-biosensor also showed a very good utility to detect nilotinib in the real samples. Finally, it might monitor novel drug compounds to interact with ds-DNA. According to these results, $In^{3+}$/NiO RLHNS is an excellent modifier for sensors and biosensors, and there is still much room for the scientific research and application development of $In^{3+}$/NiO RLHNS-based theory, materials, and devices. In the near future, commercialized nanoparticles may be incorporated into analyte detection by integrating biological elements. Advances in nano-biosensors represent reliable and positive data, so they go to the best of the future without adverse effects, and they present extraordinary discoveries and advances in research.

## Experimental Section

**Materials**. All measurements were performed at room temperature. Sigma-Aldrich Co. was chosen for purchasing salmon-sperm ds-DNA, acetic acid ($CH_3COOH$), tris-hydrochloride (tris-HCl), ethylenediaminetetraacetic acid (EDTA), sodium acetate ($CH_3COONa$), sodium hydroxide (NaOH), sodium chloride (NaCl), hydrazine ($N_2H_4$), nickel(II) chloride hexahydrate ($NiCl_2 \cdot 6H_2O$), ethylene glycol ($C_2H_6O_2$), and nilotinib·HCl. Additionally, indium(III) chloride hexahydrate ($InCl_3 \cdot 6H_2O$) was provided from Merck & Co., Inc. Each material was of analytical grade with the increased purity.

Then, the salmon-sperm ds-DNA stock solution (100 mg L$^{-1}$) was procured in the tris-HCl buffer at a pH of 7.2, and stored in the frozen state. In the next step, more diluted solutions of ds-DNA were procured with ABS at a pH of 4.8 that contained 0.02 M NaCl.
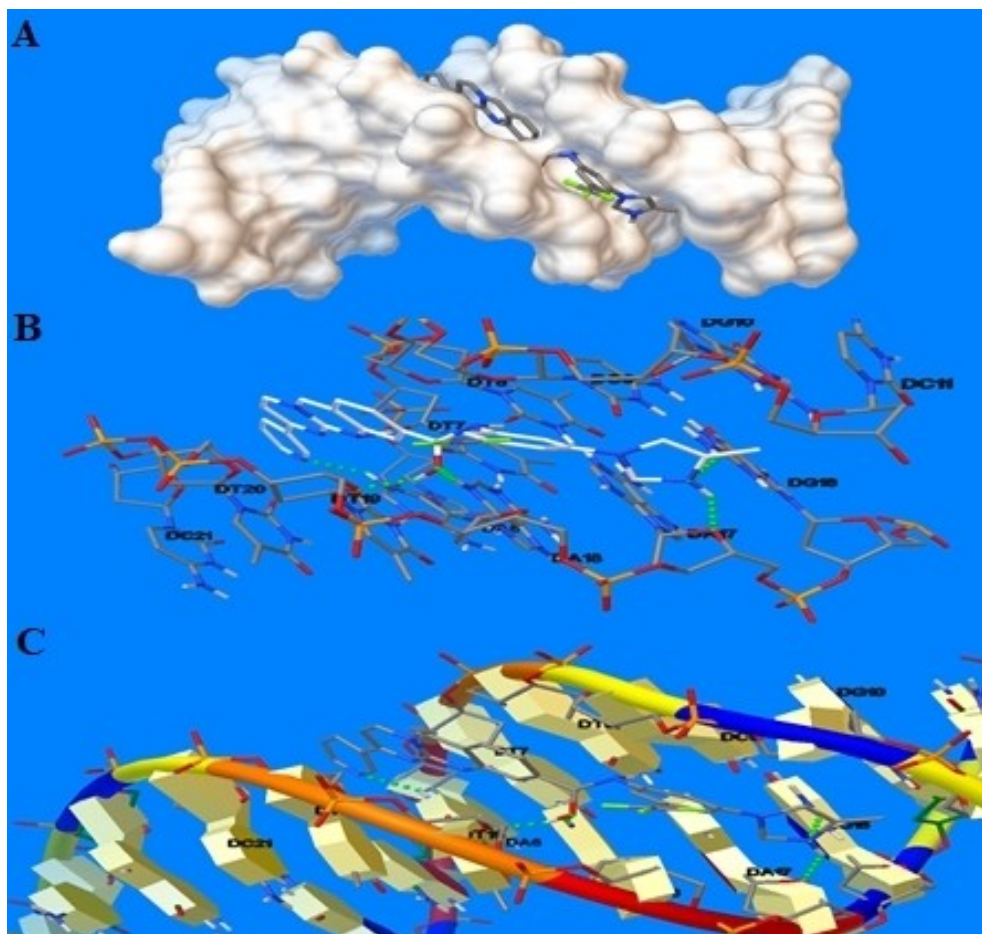
In the final step, a 1.0 mM stock solution of nilotinib was produced by the dissolution of the precisely weighed content of nilotinib in a solvent mixture of 98% ABS and 2% dimethyl sulfoxide (DMSO; $C_2H_6OS$).

**Apparatus**. A Philips analytical PC-APD X-ray diffractometer, K-α radiation ($α_2$, $λ_2 = 1.54439$ Å), and graphite monochromatic copper (Cu) radiation ($α_1$, $λ_1 = 1.54056$ Å) were utilized in the present study for the X-ray powder diffraction (XRD). A scanning electron microscope (SEM) and an energy dispersive X-ray spectroscope (KYKY & EM 3200) were applied to observe the $In^{3+}$/NiO RLHNSs. Electrochemical impedance spectra (EIS) and DPV were recorded on an SAMA 500 Electro-Analyzer with a 3-electrode system that contained a platinum (Pt) counter electrode, a silver (Ag)/AgCl reference electrode, and used CPE as the working electrode. A pH meter (pHS-3 C; Shanghai REX Instrument Factory: China) was employed for pH-value measurement, and each test was done at room temperature (ca. 25 °C).

A Shimadzu 1700 (Pharma Spec) double-beam spectrophotometer (Shimadzu Corporation; Tokyo: Japan), using quartz cuvettes of 1 cm path length at room temperature at the wavelength ranges of 200–500 nm was applied to obtain the adsorption spectra. These spectra were accordingly registered for ds-DNA-nilotinib and free ds-DNA in order to compute the binding constant of the reaction of nilotinib with ds-DNA.

An Ubbelohde-type viscometer, at 25 ± 0.1 °C in a thermo-static water-bath, was used to test viscosity. For this, nilotinib with concentrations ranging between 0 and 20 mg L$^{-1}$ (in a solvent mixture of 98% ABS and 2% DMSO) was added to the viscometer to give a specific molar ratio of nilotinib to ds-DNA so that the ds-DNA concentration remained constant at 20 mg L$^{-1}$. Following the addition of nilotinib, the solution was put aside to reach thermal equilibrium for 60 min. Afterwards, the specimen flow-time via

**ChemistryOpen**

Research Article
doi.org/10.1002/open.202100261

**Chemistry Europe**
European Chemical
Societies Publishing

**Figure 9.** (A) Nilotinib-DNA minor groove interaction; (B) and (C) geometrical disposition of nilotinib in DNA minor groove, green round dot show the hydrogen bonds between nilotinib and DNA.

capillary was measured using a digital chronometer, and relative viscosity values of ds-DNA were computed through Equation (4) in the presence and absence of nilotinib:

$$\eta/\eta_0 = (t\text{-}t_0)/(t_{ds\text{-}DNA}\text{-}t_0) \tag{4}$$

Where, $t_0$ and $t_{ds\text{-}DNA}$ refer to the flow time of 0.5 M ABS, consisting of 20 mM NaCl and ds-DNA, and $t$ represents the flow time of the ds-DNA/nilotinib mixture. The outputs are also written as $(\eta/\eta_0)^{1/3}$ plotted versus *[Nilotinib]/[ds-DNA]* ratio; $\eta$ stands for the ds-DNA relative viscosity following the addition of nilotinib, and $\eta_0$ implies the ds-DNA relative viscosity alone.

**Synthesis of the 3D Raspberry-like In³⁺/NiO Hierarchical Nanostructure.** To prepare the nanostructure, 0.028 g of indium(III) chloride hexahydrate (InCl₃·6H₂O) and 0.2 g of nickel(II) chloride hexahydrate (NiCl₂·6H₂O) were first dissolved in 20 mL of ethylene glycol, followed by achieving a green transparent solution and subsequently adding 1.5 g of 50% hydrazine mono-hydrate (N₂H₄·H₂O) while shaking, resulting in a purple solution. Additionally, 5 mL of 3 M NaOH was poured to the resulting solution and stirred at ambient temperature for 10 min. The obtained mixture was poured in a round-bottom flask (100 mL) and refluxed at a temperature of 80°C for a determined reaction time, followed by cooling down to the room temperature. The so-obtained solid product was collected and rinsed several times with water and pure ethanol, and eventually vacuum-dried in an oven for 8 h at 60°C.[37]

**Electrode Preparation.** To procure the CPEs, 0.5 g of the paste was provided with the use of a mix of 0.8 mL paraffin oil and 0.45 g graphite powder, and then pressed into a glass tube. Afterwards, a Cu wire was put on it, from the opposite end of the tube, to function as a conductor. The CPE surface was smoothened by rubbing its outer surface on a segment of paper, before being used. The modified CPEs, In³⁺/NiO RLHNSs/CPE and the NiO RLHNSs/CPE, were prepared with the same technique for which 0.05 g of the In³⁺/NiO RLHNSs and 0.05 g of NiO RLHNSs for two electrodes were added, respectively.

**Immobilizing the ds-DNA on the Surface of the Modified CPE.** In order to immobilize ds-DNA at the In³⁺/NiO RLHNSs/CPE surface, the modified CPE was submerged in the shaken 15.0 mg L⁻¹ ds-DNA, and a potential of +0.50 V was applied for 250 s. Next, the ABS was employed at the pH of 4.8 for washing the ds-DNA-modified CPE (i.e., the ds-DNA/In³⁺/NiO RLHNSs/CPE) in order to remove the un-bonded ds-DNA. Afterwards, the ds-DNA/In³⁺/NiO RLHNSs/CPE was submerged in 0.5 M ABS at the pH of 4.8, and then the potential was scanned from +600 to +1000 mV to register the guanine oxidation signal.

**Electrochemical Characterization of the Modified Surface.** Cyclic voltammograms (CV) of various modified electrodes were recorded in the redox probe solution, consisting of 5 mM ferricyanide ([Fe(CN)₆]³⁻/⁴⁻) and 0.1 M potassium chloride (KCl) by scanning the potentials between −0.5 and +0.9 V at a 50 mV s⁻¹ scan rate. EIS

**ChemistryOpen**

Research Article
doi.org/10.1002/open.202100261

**Chemistry Europe**
European Chemical
Societies Publishing

was also conducted in the redox probe solution at $+0.20$ V within a frequency range of 0.1–100 kHz, based on a 10 mV amplitude.

**Voltammetric Transduction**. DPV was registered to detect ds-DNA and to study the drug-DNA bio-interaction in the ABS at pH 4.8 for measuring the guanine oxidation signal by scanning the potential from $+0.40$ to $+1.20$ V at a pulse amplitude of 50 mV and using a $50$ mV s$^{-1}$ scan rate. The anodic current relative to the guanine oxidation at $+1.0$ V (vs. saturated calomel electrode [SCE]) was used as the analytical signal.

**Molecular Docking**. In this step, the crystal structures of the DNA duplex (entry codes 1BNA with sequence d(CGCGAATTCGCG)$_2$ dodecamer) was downloaded through the Protein Data Bank (PDB) at Brookhaven National Laboratory. To provide the most stable geometric of nilotinib, the optimization of the structure was also computed with using Gaussian 09 at the 6-31 G** level, using the B3LYP hybrid-density functional theory (DFT). Moreover, Auto-dock4.2.6 was utilized by a semi-flexible docking procedure and each nilotinib bond was set free, whereas the DNA maintained rigid. Additionally, the grid-point spacing equal to 0.375 Å as well as the grid-map with 80 Å×80 Å×80 Å points was provided. Finally, the docking showed the greatest 25,000,000 energy calculation, and thus 200 separate docking runs were done by the local search in the Lamarckian genetic algorithm (GA).[55]

**Preparation of Real Samples**. All procedures conform to the principles outlined in the declaration of Helsinki and were approved by the Ethics committee of Islamic Azad University of Kerman Branch. Informed consent from all participating subjects has been obtained.

Human blood serum and urine samples were provided from healthy volunteers and kept at $-20$°C for the assay process. Upon the transfer of a 2.5 mL volume of serum and urine into a vial, consisting of 22.5 mL ABS, a specific amount of nilotinib stock solution was poured into the vial, the mixture was transported into an electrochemical cell, and it was put aside to interact with the ds-DNA/In$^{3+}$/NiO RLHNSs/CPE until the determined time. Upon the interaction, the ds-DNA/In$^{3+}$/NiO RLHNSs/CPE was washed and put in a blank ABS, and then the DPV was recorded.

## Author Contributions

All authors contributed to the study conception and design. Material preparation and analysis were performed by Mohammad Mehdi Foroughi and Shohreh Jahani. The first draft of the manuscript was written by Mohammad Mehdi Moarefdoust and all authors commented on previous versions of the manuscript. All authors read and approved the final manuscript.

Mohammad Mehdi Moarefdoust: Writing - original draft preparation. Mohammad Mehdi Foroughi and Shohreh Jahani: Formal analysis and investigation. Mehran Moradalizadeh: Methodology. Mohammad Mehdi Motaghi: Writing - review and editing.

## Conflict of Interests

The authors declare that they have no known competing financial interests or personal relationships that could have appeared to influence the work reported in this paper.

## Data Availability Statement

Research data are not shared.

[1] C. Miguel, S. Leif, F. C. Anders, B. Magnus, *JACC: CardioOncology* **2020**, *2*, 123–126.
[2] A. E. Goda, A. E. Elisisi, S. S. Noha, M. Abdelrazik, *Toxicol. Appl. Pharmacol.* **2020**, *404*, 115185.
[3] A. Davies, A. K. Hayes, K. Knight, S. J. Watmough, M. Pirmohamed, R. E. Clark, *Leuk. Res.* **2010**, *34*, 702–707.
[4] R. A. Parise, M. J. Egorin, S. M. Christner, D. D. Shah, W. Zhou, J. H. Beumer, *J. Chromatogr. B* **2009**, *877*, 1894.
[5] S. Bouchet, E. Chauzit, D. Ducint, N. Castaing, M. Canal Raffin, N. Moore, K. Titier, M. Molimard, *Clin. Chim. Acta* **2011**, *412*, 1060.
[6] A. D'Avolio, M. Simiele, S. De Francia, A. Ariaudo, L. Baietto, J. Cusato, C. Fava, G. Saglio, F. Di Carlo, G. Di Perri, *J. Pharm. Biomed. Anal.* **2012**, *59*, 109.
[7] N. A. Lankheet, M. J. Hillebrand, H. Rosing, J. H. Schellens, J. H. Beijnen, A. D. Huitema, *Biomed. Chromatogr.* **2013**, *27*, 466.
[8] I. Andriamanana, I. Gana, B. Duretz, A. Hulin, *J. Chromatogr. B* **2013**, *926*, 83.
[9] E. Pirro, S. De Francia, F. De Martino, C. Fava, S. Ulisciani, G. R. Cambrin, S. Racca, G. Saglio, F. Di Carlo, *J. Chromatogr. Sci.* **2011**, *49*, 753.
[10] M. M. Foroughi, Sh. Jahani, M. Rajaei, *J. Electrochem. Soc.* **2019**, *166*, B1300–B1311.
[11] L. Liu, X. Zhang, Q. Zhu, K. Li, Y. Lu, X. Zhou, T. Guo, *Light-Sci. Appl.* **2021**, *10*, 181.
[12] W. B. S. Machini, N. V. Marques, A. M. Oliveira-Brett, *ChemElectroChem* **2019**, *6*, 4608–4616.
[13] M. Vakili Fathabadi, H. Hashemipour Rafsanjani, M. M. Foroughi, Sh. Jahani, N. Arefi Nia, *J. Electrochem. Soc.* **2020**, *167*, 027509.
[14] Z. Wang, H. Xiang, P. Dong, T. Zhang, C. Lu, T. Jin, K. Y. Chai, *J. Mol. Struct.* **2021**, *1224*, 129234.
[15] N. Sheibani, M. Kazemipour, S. Jahani, M. M. Foroughi, *Microchem. J.* **2019**, *149*, 103980.
[16] W. Tang, S. Wan, Z. Yang, A. E. Teschendorff, Q. Zou, C. Sahinalp, *Bioinformatics* **2018**, *34*, 398–406.
[17] C. Batchelor-McAuley, E. Kätelhön, E. O. Barnes, R. G. Compton, E. Laborda, A. Molina, *ChemistryOpen* **2015**, *4*, 224–260.
[18] S. Yan, J. Yan, D. Liu, X. Li, Q. Kang, W. You, W. He, *Theranostics* **2021**, *11*, 6833–6846.
[19] N. Arefi Nia, M. M. Foroughi, S. Jahani, *Talanta* **2020**, *222*, 121563.
[20] S. Tahmasebi, M. A. El-Esawi, Z. H. Mahmoud, A. Timoshin, H. Valizadeh, L. Roshangar, M. Varshoch, A. Vaez, S. Aslani, J. G. Navashenaq, *J. Cell. Physiol.* **2021**, *236*, 5325–5338.
[21] X. Guo, J. Wang, Y. Zhao, R. Liu, Q. Zhang, Z. Yuan, S. Sang, *Biochem. Eng. J.* **2020**, *126*, 107498.
[22] D. V. Navolotskaya, H. S. Toh, C. Batchelor-McAuley, R. G. Compton, *ChemistryOpen* **2015**, *4*, 595–599.
[23] D. Chen, M. Zhang, M. Ma, H. Hai, J. P. Li, Y. Shan, *Anal. Chim. Acta* **2019**, *1078*, 24–31.
[24] S. R. Yan, M. M. Foroughi, M. Safaei, S. Jahani, N. Ebrahimpour, F. Borhani, N. Rezaei Zade Baravati, Z. Aramesh-Boroujeni, L. K. Foog, *RSC Adv.* **2020**, *155*, 184–207.
[25] N. Jandaghi, S. Jahani, M. M. Foroughi, M. Kazemipour, M. Ansari, *Microchim. Acta* **2020**, *187*, 24–35.
[26] D. Greco, V. D'Ascanio, S. M. Sanzani, G. Avantaggiato, *Anal. Chim. Acta* **2020**, *1133*, 20–29.
[27] M. R. Rezaei Kahkha, M. Kaykhaii, G. Sargazi, B. Rezaei Kahka, *Anal. Methods* **2019**, *11*, 6168–6175.
[28] N. Arefi Nia, M. M. Foroughi, S. Jahani, M. Shahidi Zandi, N. Rastakhiz, *J. Electrochem. Soc.* **2019**, *166*, B489–B497.
[29] P. Zamani, J. G. Navashenaq, A. R. Nikpoor, M. Hatamipour, R. K. Oskuee, A. Badiee, M. R. Jaafari, *J. Controlled Release* **2019**, *303*, 223–236.
[30] S. H. Hashemi, M. Kaykhaii, A. Jamali Keikha, E. Mirmoradzehi, G. Sargazi, *BMC Chem.* **2019**, *13*, 1–10.
[31] Z. Fathi, S. Jahani, M. Shahidi Zandi, M. M. Foroughi, *Anal. Bioanal. Chem.* **2020**, *412*, 1011–1024.

ChemistryOpen

Research Article
doi.org/10.1002/open.202100261

**Chemistry**
**Europe**
European Chemical
Societies Publishing

[32] G. Sargazi, D. Afzali, A. Mostafavi, H. Kazemian, *Appl. Organomet. Chem.* **2020**, *34*, E5448.

[33] S. Tahmasebi, B. Q. Saeed, E. Temirgalieva, A. V. Yumashev, M. A. El-Esawi, J. G. Navashenaq, H. Valizadeh, A. Sadeghi, S. Aslani, M. Yousefi, *Life Sci.* **2021**, *276*, 119437.

[34] S. Munkaila, J. Bentley, K. Schimmel, T. Ahamad, S. M. Alshehri, B. P. Bastakoti, *J. Mol. Liq.* **2021**, *324*, 114676.

[35] S. Wang, Z. Yuan, W. Wu, Y. Li, H. Mi, X. Z. Ren, P. X. Zhang, L. Sun, *J. Alloys Compd.* **2021**, *862*, 158012.

[36] Y. Yajie Zhang, W. Zeng, *Mater. Lett.* **2017**, *195*, 217–219.

[37] M. M. Moarefdoust, S. Jahani, M. Moradalizadeh, M. M. Motaghi, M. M. Foroughi, *Anal. Methods* **2021**, *13*, 2396–2404.

[38] M. Ognjanović, D. M. Stanković, M. Jović, M. P. Krstić, A. Lesch, H. H. Girault, B. Antić, *Diamond Relat. Mater.* **2020**, *105*, 107785.

[39] B. B. Petković, M. Ognjanović, M. Krstić, V. Stanković, L. Babincev, M. Pergal, D. M. Stanković, *ACS Appl. Mater. Interfaces* **2020**, *3*, 4654–4662.

[40] A. Erdem, B. Kosmider, R. Osiecka, E. Zyner, J. Ochocki, M. Ozsoz, *J. Pharm. Biomed. Anal.* **2005**, *38*, 645–652.

[41] B. Dogan-Topal, B. Uslu, S. A. Ozkan, *Biosens. Bioelectron.* **2009**, *24*, 2358–2364.

[42] M. T. Carter, M. Rodriguez, A. J. Bard, *J. Am. Chem. Soc.* **1989**, *111*, 8901–8911.

[43] A. A. Ensafi, B. Rezaei, M. Amini, E. Heydari-Bafrooei, *Talanta* **2012**, *88*, 244–251.

[44] M. Pirdadeh-Beiranvand, A. Afkhami, T. Madrakian, *Anal. Bioanal. Chem.* **2020**, *412*, 1629–1637.

[45] M. Yuki, Y. Yamakawa, T. Uchida, T. Nambu, T. Kawaguchi, A. Hamada, H. Saito, *J. Clin. Lab. Anal.* **2016**, *30*, 1028–1030.

[46] M. Dziadosz, M. C. Wagner, D. B. Lipka, T. Fischer, H. Bartels, *J. Liq. Chromatogr. Relat. Technol.* **2012**, *35*, 2503–2510.

[47] H. Salem, F. A. A. Elsoud, D. Heshmat, A. Magdy, *Spectrochim. Acta Part A* **2021**, *251*, 119428.

[48] E. Kralj, J. Trontelj, T. Pajic, A. Kristl, *J. Chromatogr. B* **2012**, *903*, 150–156.

[49] C. E. Sener, B. D. Topal, S. A. Ozkan, *Anal. Bioanal. Chem.* **2020**, *412*, 8073–8081.

[50] S. Asadpour, Z. Aramesh-Boroujeni, S. Jahani, *RSC Adv.* **2020**, *10*, 31979–31990.

[51] S. U. Rehman, T. Sarwar, M. A. Husain, H. M. Ishqi, M. Tabish, *Arch. Biochem. Biophys.* **2015**, *576*, 49–60.

[52] S. S. Kalanur, U. Katrahalli, J. Seetharamappa, *J. Electroanal. Chem.* **2009**, *636*, 93–100.

[53] D. Yinhua, M. M. Foroughi, Z. Aramesh-Boroujeni, S. Jahani, M. Peydayesh, F. Borhani, M. Khatami, M. Rohani, M. Dusek, V. Eigner, *RSC Adv.* **2020**, *10*, 22891–22908.

[54] Z. Aramesh-Boroujeni, S. Jahani, M. Khorasani-Motlagh, K. Kerman, M. Noroozifar, *J. Trace Elem. Med. Biol.* **2020**, *61*, 126564.

[55] G. M. Morris, D. S. Goodsell, R. S. Halliday, R. Huey, W. E. Hart, R. K. Belew, A. J. Olson, *J. Comput. Chem.* **1998**, *19*, 1639–1662.